Organic & Biomolecular Chemistry

ROYAL SOCIETY OF CHEMISTRY

PAPER

View Article Online
View Journal | View Issue

Cite this: *Org. Biomol. Chem.*, 2025, **23**, 10391

Reactivity of an aza-dipyrrin and an aza-BODIPY motif bearing two 2-pyridyl units: an emissive NNN binding pocket

Rosinah Liandrah Gapare, [a] Roberto M. Diaz-Rodriguez, [a,b] Victoria A. Williams, [a] Mark Atwood,[a] Michael J. Cotnam,[a] James W. Hilborn,[a] Erin R. Johnson, [a] Katherine N. Robertson [c] and Alison Thompson *[a]

Received 15th October 2025,
Accepted 24th October 2025

DOI: 10.1039/d5ob01628b

rsc.li/obc

The synthesis and reactivity of an aza-dipyrrin and an aza-BODIPY motif each featuring two 2-pyridyl rings appended to the pyrrolic units are reported. The tricoordinate NNN binding domain was complexed to various metals, with Zn(II) analogues isolated and crystallographically characterised. Furthermore, the addition of alcohols across the aza-fulvenium unit provided an amino-decorated framework that served as a convenient pro-ligand for turn-on emissive metal sensing.

Introduction

Boron-containing ring systems have garnered significant attention due to their applications across diverse fields including materials science, optoelectronics, catalysis, sensors and medicinal agents.[1–3] Among these, boron complexes of dipyrrins, called BODIPYs (4,4-disubstituted-4-bora-3a,4a-diaza-s-indacenes, Fig. 1, left) shine on account of their exceptional photophysical properties. These include high fluorescence quantum yields (Φ_f), tunable absorption/emission wavelengths, and remarkable (photo)stability. Such attributes make BODIPYs indispensable in applications such as bioimaging and light-harvesting, and as sensors for environmental and biological analytes.[4]

Aza-BODIPYs are distinguished from BODIPYs by featuring a nitrogen atom at the central (*i.e., meso*) position of the dipyrrinato skeleton (Fig. 1, middle). This variation influences the photochemical properties; for example, aza-BODIPYs typically exhibit absorption and emission in the red-NIR region of the spectrum, which is a highly advantageous characteristic for biological applications. In addition, the aza-BODIPY framework (and its resultant properties) can be tuned through structural modification, such as introduction of electron-withdrawing or electron-donating aryl substituents.[5–8] The incorporation of functional aryl groups, as substituents on the dipyrrolic core, is thus an attractive approach to developing new application-focused materials.

To this end, a one-pot synthesis of 2-phenyl-4-pyridylpyrroles used 4-acetylpyridineoxime tosylate and 4′-methoxyacetophenones as starting materials, courtesy of an *in situ* Neber rearrangement that liberates a highly electrophilic 2*H*-azirine.[9] This protocol was a key component in a multi-step pathway to generate aza-dipyrrins. However, applicability was limited to aza-dipyrrinato systems bearing pyridyl units on just one of the two pyrrolic moieties, due to the approach involving reaction of an α-free pyrrole with an α-nitrosated pyrrole. As the synthesis and isolation of α-nitroso pyridyl-substituted pyrroles remains elusive,[10] this step-wise approach is unsuited to the preparation of aza-dipyrrins bearing a pyridyl unit on *each* of the pyrroles in the framework. Nevertheless, the tunability of photophysical and photochemical properties of aza-BODIPYs bearing the electron-withdrawing pyridyl motif on the pyrrolic framework offers significant allure. Furthermore, a 3,7-dipyridyl aza-dipyrrin presents a potential secondary coordinating pocket defined by the two pyridyl motifs and the *meso*-nitrogen atom, extending opportunities for tridentate NNN chelation[9,11]

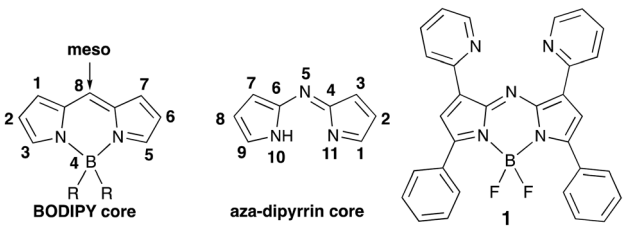

Fig. 1 BODIPY core, aza-dipyrrin core and bis(pyridyl) aza-BODIPY **1**.

[a]*Department of Chemistry, Dalhousie University, Halifax, Nova Scotia, B3H 4J3, Canada. E-mail: Alison.Thompson@dal.ca*
[b]*Department of Chemistry and Biomolecular Sciences, University of Ottawa, Ottawa, Ontario K1N 6N5, Canada*
[c]*Department of Chemistry, Saint Mary's University, Halifax, Nova Scotia, B3H 3C3, Canada*

alongside the primary pyrrole-based site through which $-BR_2$ can coordinate.[12]

In this vein, a one-pot synthesis of the bis(2-pyridyl) aza-BODIPY **1** (Fig. 1, right) from 2-phenyl-4-(2-pyridyl)pyrrole enabled the absorption and emission maxima to be determined.[13] Furthermore, binding with Hg(II) resulted in a bathochromic shift in the absorption characteristics, and identified the potential of **1** as a highly selective chemosensor. Intrigued by the potential applications[14–19] for the two complementary coordinating pockets, we targeted an improved synthesis of **1**. The potential of the neutral, tridentate NNN pocket consisting of the *meso*-nitrogen atom plus the two pyridyl nitrogen atoms, as well as the bidentate NN monoanionic pocket featuring the two pyrrolic nitrogen atoms, was also explored.

Results and discussion

Access to 1,3,7,9-tetraaryl aza-dipyrrins typically stems from the Michael addition of nitromethane to the corresponding chalcone precursors, themselves produced by aldol condensation of the corresponding aromatic aldehyde with acetophenone.[8] Accordingly, reaction of 2-pyridinecarboxaldehyde and acetophenone in the presence of $LiOH{\cdot}H_2O$ and Et_2O/EtOH, rather than *via* the reported approach involving KOH/MeOH,[20] provided 1-phenyl-3-(2-pyridyl)-2-propen-1-one. Subsequent reaction with nitromethane in the presence of Et_2NH/MeOH at reflux temperature provided the nitrobutanone **2** (Scheme 1).

A reported procedure[13] for converting nitrobutanone **2** into the key pyridyl-appended pyrrole **3** leveraged a Nef reaction, involving various sequential basic and acidic steps performed over two days to ensure condensation, deprotection and oxidation. We found this route to **3** to be procedurally heavy and inefficient, ultimately providing capricious yields upon scale-up. To address these limitations, pyrrole formation utilising sulfur and morpholine alongside an ammonia source was investigated, as this approach was reported to afford diaryl-substituted pyrroles in high yields after short reaction times.[21] Nitrobutanone **2**, morpholine, ammonium acetate, and S_8, along with ethyl acetate to aid stirring, were thus reacted for 30 minutes, which led to a dark orange-colored mixture (Scheme 1). Further addition of ethyl acetate led to precipitation of the excess sulfur; then, filtration, aqueous extraction of the mixture, and purification *via* column chromatography provided pyrrole **3** in an efficient and scalable fashion.

Attention then turned to a one-pot synthesis of aza-dipyrrin **4** (Scheme 1), *i.e.*, the formal condensation product of the reaction of 2 eq. of **3** with an NO^+ source. Following the published procedure,[13] a solution of **3** in Ac_2O/AcOH was reacted with $NaNO_2$ whilst stirring first at 0 °C and then at 80 °C. Brief examination[10] revealed that, under the reaction conditions, the nitrosopyrrole is formed immediately upon addition of $NaNO_2$ yet rapid decomposition occurs on heating. The significant degradation of the nitrosopyrrole formed *in situ* therefore impedes the formation of the desired aza-dipyrrin **4**. The reaction mixture was thus maintained at 0 °C, whereby the characteristically vivid green 2-nitroso-3,5-diarylpyrrole formed efficiently. Gradual warming to room temperature subsequently enabled the reaction of the remaining pyrrole **3** with the nitrosated species, resulting in production of **4**. Isolation involved extraction using $NaHCO_3$/CH_2Cl_2, followed by purification *via* column chromatography on neutral alumina to furnish **4** as a dark blue solid in 47% yield. A crystal structure of **4** (Fig. 2, left) confirms the two pyridyl moieties of the aza-dipyrrin flanking the nitrogen atom in the *meso* position. The aza-dipyrrinato core of **4** lies essentially coplanar with the two phenyl rings (angle between planes <6°); the two pyridyl rings, while freely rotatable, are slightly tilted *cf.* the core in the solid-state structure (up to 20°).

Although previously isolated from a one-pot reaction starting from pyrrole **3**,[13] stirring a solution of **4** in CH_2Cl_2 with $BF_3{\cdot}Et_2O$ and NEt_3 for 24 hours yielded only trace amounts of the desired aza-BODIPY **1**. However, replacing NEt_3 with $^iPr_2EtN$ and reducing the reaction time to just 30 minutes led to a significantly improved outcome. After purification *via* column chromatography on silica, the desired aza-BODIPY **1**

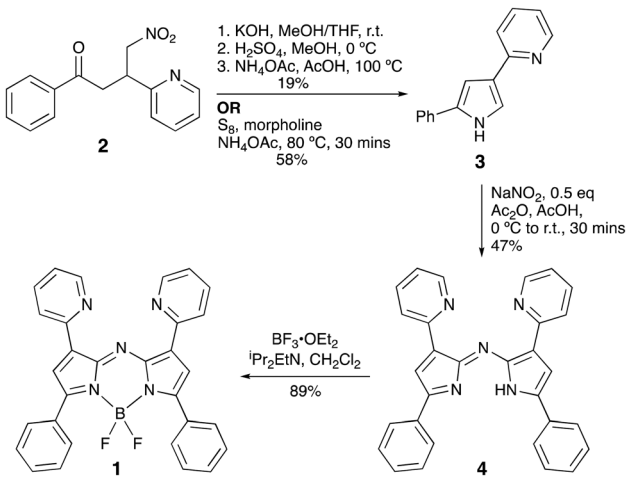

Scheme 1 Synthesis of pyridyl-substituted pyrrole, aza-dipyrrin and aza-BODIPY.

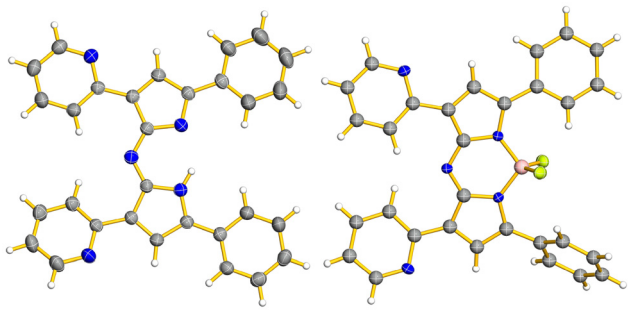

Fig. 2 Solid-state structures of bis(pyridyl) dipyrrin **4** (left) and bis-(pyridyl) F-BODIPY **1** (right). Thermal ellipsoids have been drawn with 50% probability. Only one of two possible chemically equivalent positions of the pyrrolic hydrogen atom in **4** is shown.

was isolated as a green solid in 89% yield, a success that was maintained on scales of up to 2 g. A crystal structure of **1** (Fig. 2, right) confirmed the presence of the $-BF_2$ unit. Unlike the corresponding ligand, the aryl substituents around the aza-dipyrrinato core of **1** are notably more deviated from coplanarity (by up to 50° for the phenyl substituent at C1, and 17–25° for the others).

With reliable syntheses in hand, attention turned to investigating the reactivity of the aza-BODIPY **1** and the dipyrrin **4**. The presence of pyridyl groups on the framework offer the opportunity to quench emission *via* photoinduced electron transfer, leading us to explore the effects of methylation. Indeed, the redox properties of *N*,*N*′-4,4-dialkyl bipyridinium systems (viologens) have been extensively studied for use in diverse fields like electrocatalysis, electro- and photochromism, herbicides, and energy storage systems.[22–25] Treatment of the aza-BODIPY **1** with CH_3I resulted in a yellowing of the dark green solution alongside formation of an orange precipitate. The precipitate, collected by filtration, was identified as the dimethylated analogue **5** (Fig. 3, left). The filtrate was concentrated to provide a green oil, which was not further purified; analysis of the corresponding NMR data confirmed methylation at just one of the pyridyl nitrogen atoms. The NMR spectra of **5** are representative of an unsymmetrical structure, presumably as a result of the two alkylated pyridyl groups exhibiting different conformational preferences. Protonation of **1**, to provide the triflate salt **6a** (Fig. 3, right) and the perchlorate salt **6b**, also demonstrated reactivity at the pyridyl nitrogen atoms as confirmed by X-ray crystallography (Fig. 4 and SI).

Efforts to determine the pK_a of **1** using absorption spectroscopy were complicated by evident solvatochromic behaviour. The dimethylated analogue **5** also exhibited solvatochromicity: a solution of **5** in MeCN was green in colour; solutions in MeOH, DMSO and DMF were orange; and those in THF and acetone were yellow (Fig. S10). Solvent-dependent behaviour was further evident in NMR spectra, as illustrated in Fig. 5.

The photophysical properties of the dipyridyl-containing aza-dipyrrinato constructs are presented in Table 1. Complexation of **4** with $-BF_2$ to form the aza-BODIPY **1** results in an anticipated red shift in absorbance maximum, and a corresponding shift in emission along with a significant increase in quantum yield. The methylated analogue **5** retains the absorption characteristics of the BODIPY **1** and, unsurprisingly, methylation results in quenched emission.

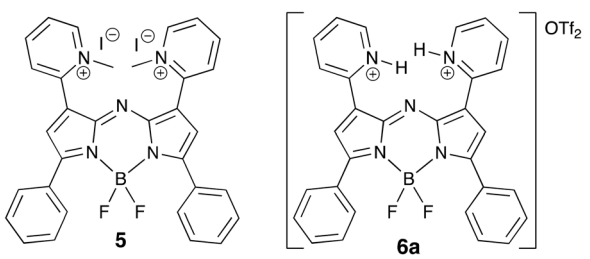

Fig. 3 Methylated and protonated analogues of **1**.

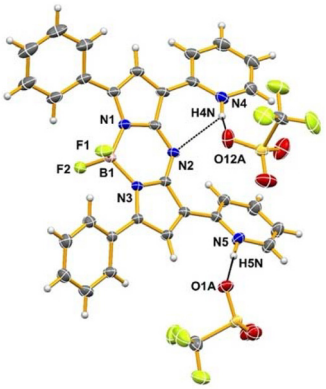

Fig. 4 Structure of cation **1** in **6a** showing its hydrogen bonding (dashed lines). There is a second unique cation in the structure, nearly related by inversion symmetry, which has been omitted for clarity. Disorder of the anions has also been omitted. Thermal ellipsoids have been drawn at the 50% probability level. Hydrogen atoms are included (most are not labelled).

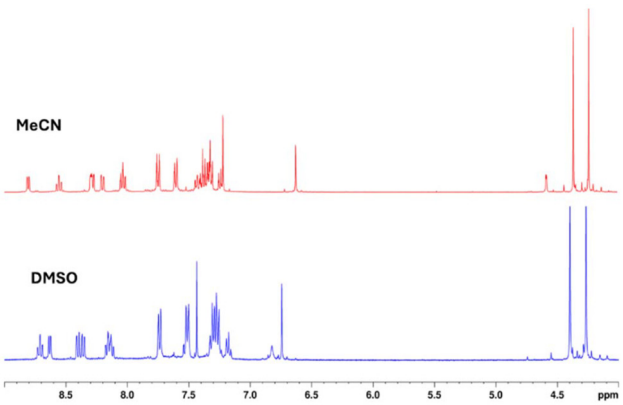

Fig. 5 ^{1}H NMR spectra of compound **5** in DMSO (bottom) and MeCN (top).

Encouraged by the propensity of the tridentate NNN pocket towards methylation and protonation, the coordination reactivity of **1** was next explored. With a view to evaluating the potential complexation of lanthanides within the tridentate pocket, a solution of **1** in $CHCl_3$/MeOH was reacted with 1 eq. $Er(NO_3)_3{\cdot}5H_2O$, as shown in Scheme 2. Over the course of four days the colour gradually changed from deep green, through yellowish-green, and eventually to a deep blue solution from which some solid material precipitated. After this time, a small number of orange crystals were obtained, isolated *via* filtration and washed with pentane.

The ^{1}H NMR spectrum (Fig. 6, top) of a solution of this material in CD_3CN displayed a methyl signal at 3.5 ppm, suggestive of the presence of a methoxy group. Furthermore, two singlets each integrating to 1H, and with chemical shifts corresponding to a H-atom on the carbon backbone of a

Table 1 Photophysical properties

Compound	Solvent	$\lambda_{max,abs}$ [a] (nm)	ε (M^{-1} cm^{-1})	$\lambda_{max,em}$ [b] (nm)	Stokes shift (nm)	Φ_f
1	CH_2Cl_2	664	82 000	703	39	0.27
4	CH_2Cl_2	604	29 000	664	60	0.004
5	MeCN	664	44 000	706	42	0.04
6	MeCN	634	11 000	731	97	0.18
7	MeCN	438	9 000	676	238	0.03
8	MeCN	438	3 000	704	266	0.02
1-Zn(ClO$_4$)$_2$	MeCN	694	73 000	745	51	0.13
4-Zn(ClO$_4$)$_2$	MeCN	648	34 000	712	64	0.006

[a] Wavelength of maximum absorbance. [b] Wavelength of maximum fluorescence emission.

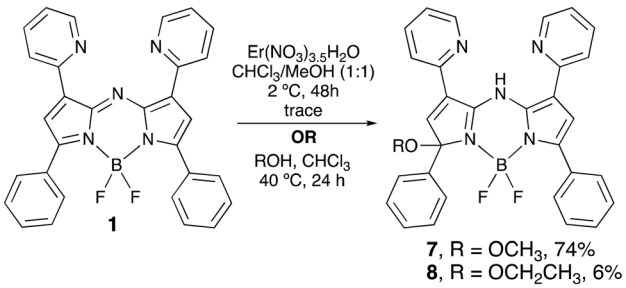

Scheme 2 Addition of methanol across the azafulfenium moiety of **1**.

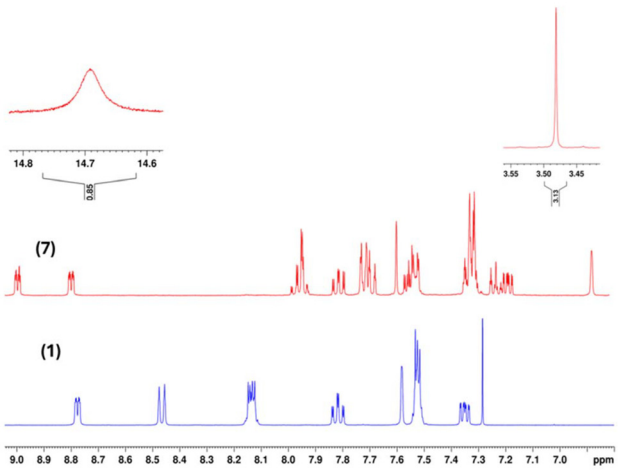

Fig. 6 ^{1}H NMR spectra of **1** (bottom) and **7** (top) in CD_3CN.

pyrrolic ring and a vinylic hydrogen atom, provided evidence suggestive of desymmetrisation *cf.* **1**. The peaks corresponding to the aryl protons attributable to the pyridyl rings further supported desymmetrisation. The ^{1}H NMR spectrum featured a signal at 14.7 ppm, likely indicative of a highly deshielded NH unit.

Given these data, and the sharpness of the NMR signals, the isolated material was evidently not the expected BODIPY-based lanthanide complex. Given that the $-BF_2$ motif remained coordinated to the pyrrolic nitrogen atoms, as confirmed by ^{11}B and ^{19}F NMR spectroscopy, it seemed reasonable to conclude that the observed N*H* signal originated with the *meso*-nitrogen atom: as such, addition of methanol across the azafulvenium moiety of **1**, to form **7**, was suspected (Scheme 2), and was confirmed by an X-ray crystal structure (Fig. 7) and ESI$^+$ mass spectrometry.

Presumably, the Lewis acidic nature of $Er(NO_3)_3{\cdot}5H_2O$, and/or the Brønsted acidity of the methanolic solution, catalysed the addition of alcohol to form **7**. Pleasingly, simply stirring a methanolic solution of **1** at 40 °C for 24 h (Scheme 2) resulted in formation of **7** in a much-improved yield. The ethanol adduct **8** was obtained *via* similar means (Scheme 2) and the structure confirmed *via* X-ray crystallographic analysis (see SI), although only a trace amount of the corresponding adduct was isolated when **1** was stirred with isopropanol. Addition of alcohol across the azafulvene moiety of the aza-BODIPY **1** results in a colour change from deep green to orange, with the absorption maximum at 438 nm (Table 1).[26] Furthermore, as a consequence of the demise of the fully conjugated dipyrrinato framework (Fig. S21), the fluorescence emission of **1** is, unsurprisingly, lost upon formation of **7** and **8**. Anticipating that emission might be restored upon complexation, the optical behaviour of **7** was studied in the presence of Mn^{2+}, Fe^{3+}, NH_4^+, Ni^{2+}, Cu^{2+}, Zn^{2+}, Na^+, K^+, Mg^{2+}, Fe^{2+}, Ca^{2+}, Al^{3+} and Sb^{3+}. Upon the addition of Zn^{2+}, Sb^{3+} or Al^{3+} to a solution of **7** in MeCN, significantly red-shifted absorption properties were observed (Fig. S28); the addition of the other metal ions

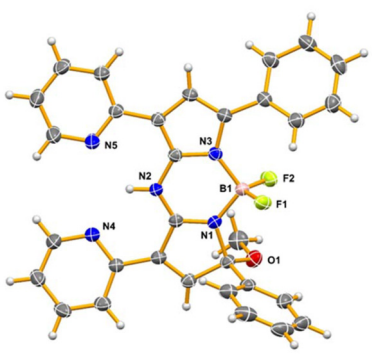

Fig. 7 Structure of compound **7** with the solvent omitted for clarity. Thermal ellipsoids have been drawn at the 50% probability level. Hydrogen atoms are included (not labelled).

resulted in less dramatic changes. Intriguingly, addition of solutions of Zn^{2+} or Sb^{3+} to a solution of **7** restored emission (Fig. 8) and resulted in maxima at 745 nm (excitation at 600 nm), *i.e.* bathochromically shifted *cf.* the aza-BODIPY **1**. In contrast, the addition of Al^{3+} to a solution of **7** resulted in an emission maximum at 660 nm. Addition of the other metal ions effected only insignificant changes in emission or spectral position. Thus, the addition of select metal ions clearly results in complexation within the NNN tridentate pocket, and the $-BF_2$ unit originating with **7** is maintained upon the addition of the metal salts. The solutions containing Zn^{2+} and Sb^{3+} both absorb in the near-IR region ($\lambda_{max,abs}$ = 694 nm for the solution containing **7** and Zn^{2+}; $\lambda_{max,abs}$ = 684 nm for the solution containing **7** and Sb^{3+}), presumably as a result of enhanced coplanarisation of the aza-dipyrrinato core and the pyridyl units. Impressively, the effect of this planarisation on the absorption maxima is greater than that of the red-shifting observed upon formation of the aza-BODIPY **1** from the aza-dipyrrin **4**.

Given the NNN-tridentate binding opportunities offered by the two pyridyl units and the *meso*-nitrogen of the aza-dipyrrinato system, the potential of **7** for metal ion sensing was explored.[13,26–31] The addition of increasing concentrations of $Zn(ClO_4)_2$ in MeCN to a solution of **7** in MeCN was monitored using absorbance (Fig. 9) and emission (Fig. S30) spectroscopies. As the concentration of Zn^{2+} increased, emission at 745 nm increased concurrently. The addition of Zn^{2+} to a solution of **7** in MeCN results in a dramatic enhancement in absorption in the 600–750 nm range (Fig. 9); similar behaviour is observed in the emission characteristics (Fig. S30). Importantly, **7** has negligible absorption and emission in the 600–750 nm range, and so detection of metal ions using **7** constitutes a turn-on sensor. This characteristic also renders **7** a superior metal ion sensor than the fluorescent aza-BODIPY **1**.[13]

To provide a rationale for the complexation chemistry observed for this system, the geometry of the putative BODIPY complex ion with Zn^{2+} (*i.e.* **1-Zn$_2$**) was optimised using B86bPBE0-XDM/lightdense[32] and the ZORA scalar relativistic correction using the FHI-aims program.[33] The optimised geometry demonstrated a planar binding arrangement about Zn, with a Zn–$N_{pyridyl}$ bond length of 1.926 Å and Zn–N_{meso} bond lengths of 1.921 Å (Fig. 10).

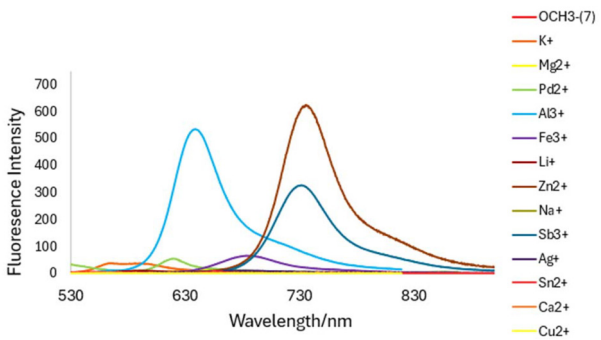

Fig. 8 Emission spectra of solutions of **7** in MeCN (0.13 mM) upon the addition of 20 eq. of metal ions (λ_{ex} = 600 nm).

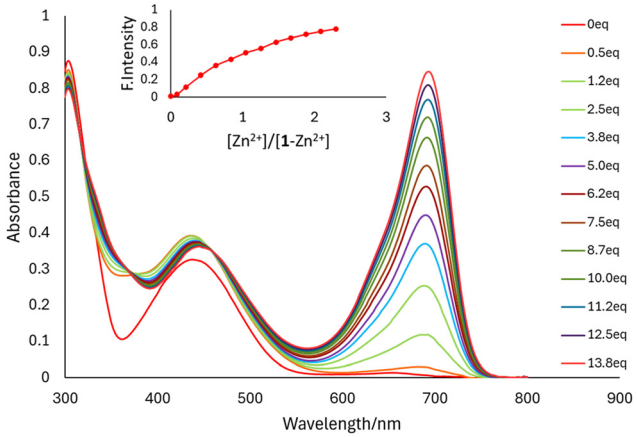

Fig. 9 Changes in absorption spectra of a solution of **7** in MeCN (5 μM) upon the addition of $Zn(ClO_4)_2$ (0.5–14 eq.) in MeCN. *Inset*: plot of absorbance at 664 nm as a function of $[Zn^{2+}]$.

While previous studies have explored the metal-sensing properties of the aza-BODIPY **1**,[13] there are no reports to date regarding the isolation and characterisation of its complexes. X-ray diffraction analysis of a single crystal grown from the mixture resulting from the reaction of **7** with $Zn(ClO_4)_2$ in MeCN revealed the complex **1-Zn(ClO$_4$)$_2$** (Fig. 11). Evidently, the methoxy adduct **7** acts as a proligand, complexing the metal with loss of methanol upon the addition of $Zn(ClO_4)_2$. In agreement with the computational predictions, the metal ion is complexed by the neutral tridentate NNN binding pocket of **1**. However, the Zn^{2+} centre was found to be further coordinated by acetonitrile and one perchlorate ion (with the second perchlorate ion remaining uncoordinated), deviating the metal ion from coplanarity with the donor atoms in the NNN pocket. Given that **7** is non-emissive at >600 nm, the sensing ability of the proligand is realised by turn-on emission through *in situ* generation of the emissive aza-BODIPY motif. Quenching of the reaction mixture containing **1-Zn(ClO$_4$)$_2$** with water and extraction into CH_2Cl_2 revealed a mild instability to aqueous conditions manifesting as a (partial) loss of the $-BF_2$ unit, which was confirmed crystallographically (see SI).

The aza-dipyrrin **4** also complexes Zn^{2+} upon reaction with $Zn(ClO_4)_2$, again positioning the metal in the neutral triden-

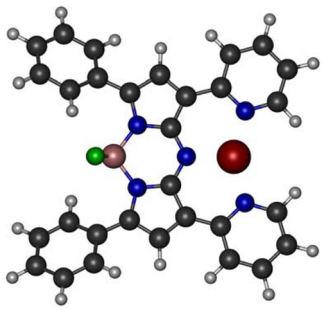

Fig. 10 DFT-optimised geometry of the putative Zn^{2+} complex of **1**.

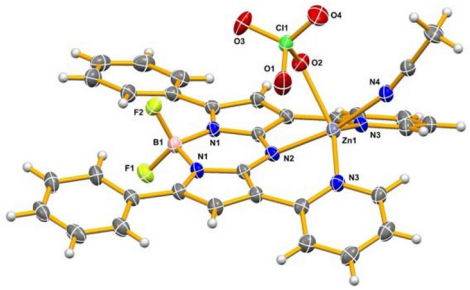

Fig. 11 Structure of the cation in **1-Zn(ClO$_4$)$_2$**. Only one half of the cation is unique. The non-coordinating anion and the disorder of the coordinated perchlorate group have been omitted for clarity. Thermal ellipsoids have been drawn at the 50% probability level. Hydrogen atoms are included but have not been labelled.

tate NNN pocket (see SI). Intriguingly, complexation of metals with **4** *via* the NNN pocket leaves the bidentate aza-dipyrrinato binding motif available for further complexation, and enables future exploration of the sensing properties of this versatile pyridyl-appended dipyrrinato framework.

Conclusions

A refined synthetic route to the 3,7-(2-pyridyl)-appended aza-BODIPY **1** is presented herein, accompanied by isolation and characterisation of the parent aza-dipyrrin **4**. The chemical reactivity of the aza-dipyrrin **4** and the aza-BODIPY **1** was evaluated, including methylation and protonation of the pyridyl nitrogen atoms. Most importantly, it is demonstrated that **1** can add unhindered alcohols across the azafulvene unit, and that the resulting non-emissive adducts sense metal complexation in a turn-on-emissive manner. Consequently, we report herein the first isolation, characterisation and solid-state structure of a complex featuring a metal ion in the neutral tridentate NNN pocket, which consists of the two pyridyl nitrogen atoms and the *meso*-nitrogen atom of the aza-dipyrrinato framework. Of further note, complexation of **4** *via* the neutral tridententate NNN binding pocket leaves the bidentate aza-dipyrrinato binding motif available for further complexation, and a variety of potential applications can therefore be envisioned.

Author contributions

Conceptualisation: RLG, RD-R and AT. Funding acquisition: AT. Investigation: RLG, RD-R, VAW, MA, MJC, JWH, ERJ and KNR. Project administration: AT. Supervision: AT. Writing – original drafts: RLG and AT. Writing – review & editing: RLG, RD-R, VAW, MA, JWH, ERJ, KNR and AT.

Conflicts of interest

There are no conflicts to declare.

Data availability

Data supporting this article have been included as part of the supplementary information (SI). Supplementary information: synthesis details and characterisation data. See DOI: https://doi.org/10.1039/d5ob01628b.

CCDC 2494132, 2494133 and 2486550–2486557 contain the supplementary crystallographic data for this paper.[34a–j]

Acknowledgements

We thank Dr Michael Lumsden and Mr Xiao Feng (both at Dalhousie University) for sharing their expertise in NMR spectroscopy and mass spectrometry, respectively. This work was supported, in part, by NSERC of Canada *via* Discovery Grants and the CREATE Training Program in BioActives (510963). This work was enabled, in part, thanks to funding from the Canada Research Chairs Program (funding reference number 950-232829). This research was enabled, in part, by funding from the Canada Foundation for Innovation (JELF 39824) and Research Nova Scotia (Research Opportunities Fund 2020-1208).

References

1 R. J. Grams, W. L. Santos, I. R. Scorei, A. Abad-García, C. A. Rosenblum, A. Bita, H. Cerecetto, C. Viñas and M. A. Soriano-Ursúa, *Chem. Rev.*, 2024, **124**, 2441–2511.
2 Y. Su and R. Kinjo, *Chem. Soc. Rev.*, 2019, **48**, 3613–3659.
3 Z. Huang, S. Wang, R. D. Dewhurst, N. V. Ignat'ev, M. Finze and H. Braunschweig, *Angew. Chem., Int. Ed.*, 2020, **59**, 8800–8816.
4 R. L. Gapare and A. Thompson, *Chem. Commun.*, 2022, **58**, 7351–7359.
5 C. Schäfer, J. Mony, T. Olsson and K. Börjesson, *J. Org. Chem.*, 2022, **87**, 2569–2579.
6 A. Bessette and G. S. Hanan, *Chem. Soc. Rev.*, 2014, **43**, 3342–3405.
7 J. K. G. Karlsson and A. Harriman, *J. Phys. Chem. A*, 2016, **120**, 2537–2546.
8 Y. Ge and D. F. O'Shea, *Chem. Soc. Rev.*, 2016, **45**, 3846–3864.
9 C. Liu, Y. Jin, X. Ji, W. Zhao and X. Dong, *Chem. – Eur. J.*, 2022, **28**, e202201503.
10 E. B. Brown, R. L. Gapare, J. W. Campbell, A. Alkaş, S. Sequeira, J. W. Hilborn, S. M. Greening, K. N. Robertson and A. Thompson, *Org. Biomol. Chem.*, 2024, **22**, 6122–6128.
11 C. Liu, C. Liu, X. Ji, W. Zhao and X. Dong, *J. Med. Chem.*, 2024, **67**, 15908–15924.
12 E. J. González Lopez, A. M. Sarotti and D. A. Heredia, *Org. Lett.*, 2025, **27**, 8602–8606.
13 A. Coskun, M. D. Yilmaz and E. U. Akkaya, *Org. Lett.*, 2007, **9**, 607–609.

14 W. Wu, H. Guo, W. Wu, S. Ji and J. Zhao, *J. Org. Chem.*, 2011, **76**, 7056–7064.
15 Y. Chen, J. Zhao, L. Xie, H. Guo and Q. Li, *RSC Adv.*, 2012, **2**, 3942–3953.
16 M. D. Ward, *Coord. Chem. Rev.*, 2010, **254**, 2634–2642.
17 A. D'Aléo, F. Pointillart, L. Ouahab, C. Andraud and O. Maury, *Coord. Chem. Rev.*, 2012, **256**, 1604–1620.
18 W. Thor, H.-Y. Kai, Y.-H. Yeung, Y. Wu, T.-L. Cheung, L. K. B. Tam, Y. Zhang, L. J. Charbonnière, P. A. Tanner and K.-L. Wong, *JACS Au*, 2024, **4**, 3813–3822.
19 E. Hemmer, N. Venkatachalam, H. Hyodo, A. Hattori, Y. Ebina, H. Kishimoto and K. Soga, *Nanoscale*, 2013, **5**, 11339–11361.
20 A. Rosas-Sánchez, R. A. Toscano, J. G. López-Cortés and M. C. Ortega-Alfaro, *Dalton Trans.*, 2014, **44**, 578–590.
21 M. Adib, N. Ayashi, F. Heidari and P. Mirzaei, *Synlett*, 2016, 1738–1742.
22 C. L. Bird and A. T. Kuhn, *Chem. Soc. Rev.*, 1981, **10**, 49–82.
23 M. Kathiresan, B. Ambrose, N. Angulakshmi, D. E. Mathew, D. Sujatha and A. M. Stephan, *J. Mater. Chem. A*, 2021, **9**, 27215–27233.
24 B. Ambrose, R. Naresh, S. Deshmukh, M. Kathiresan and P. Ragupathy, *Energy Fuels*, 2023, **37**, 18226–18242.
25 A. Iriel, J. M. Novo, G. B. Cordon and M. G. Lagorio, *Photochem. Photobiol.*, 2014, **90**, 107–112.
26 F.-Z. Li, Z. Wu, C. Lin, Q. Wang and G.-C. Kuang, *Results Chem.*, 2022, **4**, 100384.
27 J. Du, J. Fan, X. Peng, H. Li, J. Wang and S. Sun, *J. Fluoresc.*, 2008, **18**, 919–924.
28 X. Peng, J. Du, J. Fan, J. Wang, Y. Wu, J. Zhao, S. Sun and T. Xu, *J. Am. Chem. Soc.*, 2007, **129**, 1500–1501.
29 L. Zeng, E. W. Miller, A. Pralle, E. Y. Isacoff and C. J. Chang, *J. Am. Chem. Soc.*, 2006, **128**, 10–11.
30 B. Wang, P. Li, F. Yu, P. Song, X. Sun, S. Yang, Z. Lou and K. Han, *Chem. Commun.*, 2013, **49**, 1014–1016.
31 Y. Wu, X. Peng, B. Guo, J. Fan, Z. Zhang, J. Wang, A. Cui and Y. Gao, *Org. Biomol. Chem.*, 2005, **3**, 1387–1392.
32 A. J. A. Price, A. Otero-de-la-Roza and E. R. Johnson, *Chem. Sci.*, 2023, **14**, 1252–1262.
33 V. Blum, R. Gehrke, F. Hanke, P. Havu, V. Havu, X. Ren, K. Reuter and M. Scheffler, *Comput. Phys. Commun.*, 2009, **180**, 2175–2196.
34 (*a*) CCDC 2494132: Experimental Crystal Structure Determination, 2025, DOI: 10.5517/ccdc.csd.cc2pqbwn; (*b*) CCDC 2494133: Experimental Crystal Structure Determination, 2025, DOI: 10.5517/ccdc.csd.cc2pqbxp; (*c*) CCDC 2486550: Experimental Crystal Structure Determination, 2025, DOI: 10.5517/ccdc.csd.cc2pgg9y; (*d*) CCDC 2486551: Experimental Crystal Structure Determination, 2025, DOI: 10.5517/ccdc.csd.cc2pggbz; (*e*) CCDC 2486552: Experimental Crystal Structure Determination, 2025, DOI: 10.5517/ccdc.csd.cc2pggc0; (*f*) CCDC 2486553: Experimental Crystal Structure Determination, 2025, DOI: 10.5517/ccdc.csd.cc2pggd1; (*g*) CCDC 2486554: Experimental Crystal Structure Determination, 2025, DOI: 10.5517/ccdc.csd.cc2pggf2; (*h*) CCDC 2486555: Experimental Crystal Structure Determination, 2025, DOI: 10.5517/ccdc.csd.cc2pggg3; (*i*) CCDC 2486556: Experimental Crystal Structure Determination, 2025, DOI: 10.5517/ccdc.csd.cc2pggh4; (*j*) CCDC 2486557: Experimental Crystal Structure Determination, 2025, DOI: 10.5517/ccdc.csd.cc2pggj5.